Numerical Simulation of 3D Turbulent Flow Separation around a Spheroid

李　信亨　運輸省船舶技術研究所　〒181-0004　東京都三鷹市新川 6-38-1 E-mail:shrhee@srimot.go.jp
日野孝則　運輸省船舶技術研究所　〒181-0004　東京都三鷹市新川 6-38-1 E-mail:hino@srimot.go.jp

Turbulent separated flows around a *6:1* prolate spheroid are investigated using an unstructured grid CFD method. The RANS equations are solved for incompressible viscous flows. The artificial compressibility is introduced in the continuity equation and cell-centered finite-volume method on unstructured grid is used for spatial discretization. The Spalart-Allmaras one-equation turbulence model is employed for the Reynolds stress. The computational results are compared with experimental data and the physics of three-dimensional turbulent flow separation is confirmed. Two angles of attack is considered and the effects are investigated. The modification of the Spalart-Allmaras model is added to improve the performance for the vortical flow structure.

1. INTRODUCTION

The flow separation around a three-dimensional (3D) body is one of the most interesting and challenging problems in fluid mechanics. The separated flow around a body results in many phenomena in aero- and hydrodynamics, such as the drag increase, lift loss, and unsteady fluctuation, etc. Therefore, it is of great importance for designers to understand and predict flow separation around a surface ship, submarine, airplane, or other fluid dynamic devices.

The separation can be defined as the entire process of departure or breakaway, or the breakdown of boundary layer flow[1]. Researches on two-dimensional (2D) flow separation have provided basic and important characteristics of the phenomenon. However, 3D flow separation is quite different from its 2D counterpart in that, primarily,: the type of separation varies with Reynolds number, angle of attack, and body geometry; the cross flow separation occurs and exerts great influence on the post-separation region and wake; and the flow reversal and zero-shear point are not always present with the separation.

Considering the current status of computational fluid dynamics (CFD) techniques and the increasing demands for a better prediction method for 3D turbulent flow separation, the objectives of the present study are: (a) to apply an unstructured grid CFD method to 3D flow separation around a body of revolution; (b) to validate the computational results by comparison with theoretical study and experimental data; and (c) to investigate the effects of angle of attack on the separation pattern and forces and moments. Although the geometry of interest in the present study is simple, an unstructured grid method, which is regarded as an alternative to structured grid methods for complex geometry problems, is employed here because further application to practical problems is the ultimate goal in mind.

Numerical method employed is presented next followed by results and concluding remarks.

2. NUMERICAL METHOD

The governing equations are 3D RANS equations for incompressible flow. In order to couple a pressure field with the corresponding velocity one, artificial compressibility is introduced into the continuity equations. The finite volume method is adopted for spatial discretization. Flow variables are stored at the center of each cell. For inviscid fluxes, the second order upwind scheme based on the flux-difference splitting of Roe[2] with the MUSCL approach is employed. Viscous fluxes are evaluated by the second order central scheme. The time derivative terms are discretized using Euler backward and the second order backward scheme for pseudo- and physical time derivative terms, respectively. After the discretization, the linear equation is solved by the Symmetric Gauss-Seidel iteration. The pseudo-time iteration continues until the averaged pressure residual between pseudo-time iteration, i.e., continuity equation imbalance, reaches convergence criterion or the iteration number reaches its pre-set maximum. The eddy viscosity for turbulent flow calculations is obtained by the one-equation Spalart-Allmaras model[3] and its modification proposed by Dacles-Mariani et al.[4]. For detailed description of numerical methods, readers are recommended to refer to Hino[5] and Rhee and Hino[6].

3. RESULTS

The solution domain looks like a half of an egg, i.e., a half-domain, with extent $-1.5 \le x/L \le 4.5$, $-2.0 \le y/L \le 2.0$, $0 \le z/L \le 2.0$ and the origin at the nose of the spheroid. In order to exploit the simplicity of the geometry, a structured grid with hexahedral cells, i.e., (streamwise×normal×circumferential) = *(90×64×60) = 345,600* cells, was generated. The average minimum spacing in the normal direction is about 1×10^{-5}. Note that in the results presentation, ϕ is $0°$ at the symmetry plane on the windward side and $180°$ on the opposite side. No-slip condition with zero-gradient pressure is imposed on the solid wall and a symmetry condition is applied on the symmetry plane. On the outer boundary, the free-stream condition with a specified angle of attack (α) is given up to *x/L=0.0* and a simple extrapolation is done on the remaining outer boundary. The computational conditions are $\alpha=10°$, $20°$, and Reynolds number $Re=U_0L/\nu=4.2\times10^6$.

All the results of turbulent flow are computed using the modified SA model and compared with experimental data[7]. The correction parameter for ν_t production term (C_{vor}) in the turbulence model is set to be *20* based on the authors' experience in CFD simulations for surface ship hull forms. The transition to turbulent flow is forced at *x/L=0.2* following the experiments.

Table 1. Lift, drag, and yaw moment coefficients.

α (°)	10	20
$C_{D,total}$	4.71×10^{-4}	1.22×10^{-3}
$C_{D,pressure}$	1.53×10^{-4}	8.70×10^{-4}
$C_{D,friction}$	3.18×10^{-4}	3.47×10^{-4}
$C_{L,total}$	7.85×10^{-4}	2.84×10^{-3}
$C_{L,pressure}$	6.81×10^{-4}	2.64×10^{-3}
$C_{L,friction}$	1.05×10^{-4}	2.02×10^{-4}
$M_{z,total}$	-8.86×10^{-4}	-1.35×10^{-3}
$M_{z,pressure}$	-8.80×10^{-4}	-1.34×10^{-3}
$M_{z,friction}$	-5.80×10^{-6}	-8.00×10^{-6}

Table 1 presents the components of drag $\left(C_D = Drag \Big/ \frac{1}{2}\rho U_0^2 L^2\right)$, lift $\left(C_L = Lift \Big/ \frac{1}{2}\rho U_0^2 L^2\right)$, and yaw (z-axis) moment

$\left(M_z = Yaw\,moment \Big/ \frac{1}{2}\rho U_0^2 L^3 \right)$ coefficients at the two α's. As Matsumura et al.[8] pointed out, C_D and C_L increase non-linearly with increasing α, mainly due to the large increase of pressure component, which is subject to the separation pattern.

The skin friction lines on the whole body are presented in Fig. 1. The inflected lines on the fore-body are due to the turbulence stimulation. The general pattern is similar to that for laminar flow[6]; however, the separation lines are moved to the leeward and backward, which is analogous to the delayed separation on a sphere in turbulent flow. Also the weak secondary separation $\alpha=10°$ is consistent with the report of Chesnakas and Simpson[7].

Fig. 2 presents the pressure coefficient C_p contours on the whole body. Compared to that for laminar flow, the peak value and the favorable/adverse pressure gradients in the streamwise and circumferential directions are larger in the turbulent flow. Also noteworthy at $\alpha=20°$ is the inflection in contour lines near the primary and secondary separation lines, which confirms the relations between the pressure, pressure gradient, and separation line[9].

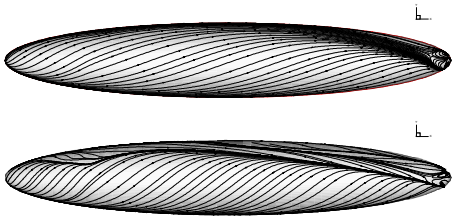

$\alpha=10°$ (upper); $\alpha=20°$ (lower)
Fig. 1 Skin friction lines on the whole body.

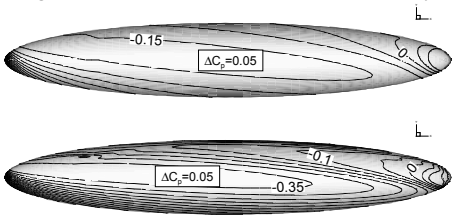

$\alpha=10°$ (upper); $\alpha=20°$ (lower)
Fig. 2 C_p contours on the whole body.

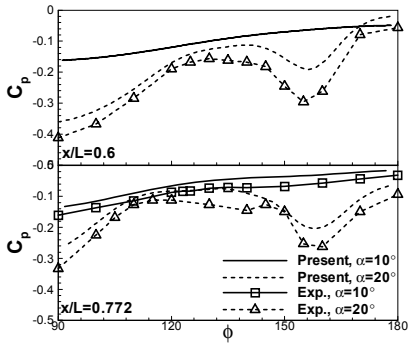

Fig. 3 Comparison of pressure coefficient.

The C_p at $x/L=0.600$ and 0.772 is compared with the experimental data and presented in Fig. 3. The agreement is qualitatively good, and the primary $(\phi=123°)$ and secondary $(\phi=145°)$ separation locations can be detected by the pressure gradient, since C_p becomes almost flat past the separation. However, the present results show somewhat consistent difference from the experimental data, and the reason may be due to a difference in the reference pressure. The increasing difference with the increasing α is expected from the fact that the turbulence anisotropy increases with increasing α and x/L[7], i.e., due to the strong correlation between turbulence anisotropy, separation line, vortical flow structure, and pressure field.

Fig. 4 presents the skin friction coefficient C_f at $x/L=0.400$, 0.600 and 0.772, and the comparison with the experimental data. It should be noted here that C_f from the experiment was calculated using the velocity profiles fitted to a Spalding type wall law, and it may cause the consistent difference in the comparison as shown in the figure. As for C_p, the agreement is qualitatively good, and the locations of primary and secondary separation are well detected by the local minima of C_f lines[9]. However, the peak values for $\alpha=20°$ are under-estimated, which is again attributed to the strong turbulence anisotropy.

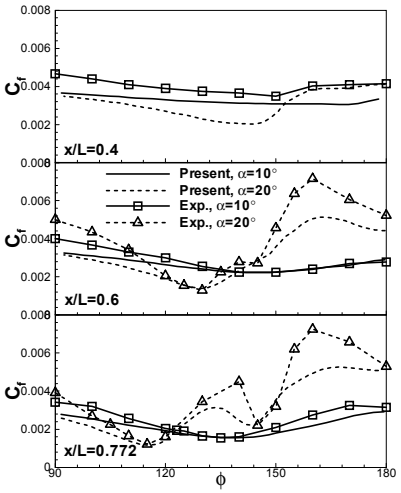

Fig. 4 Comparison of skin friction coefficient.

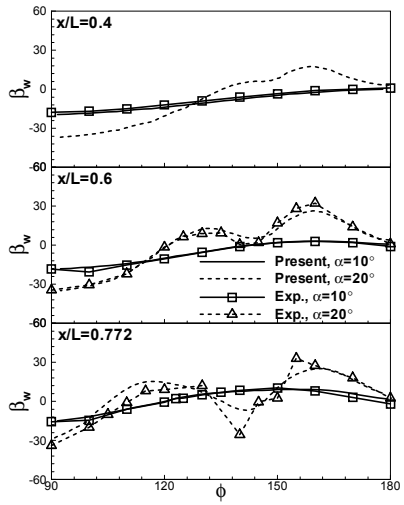

Figure 5. Comparison of flow angle.

Fig. 5 presents the wall-flow angle β_w, i.e., the direction of the flow at the wall relative to the streamwise direction, at $x/L=0.400$, 0.600 and 0.772, and the comparison with the experimental data. Since the wall-flow is sensitive to minor variations inside separated regions, it is rather difficult to correctly estimate β_w. The present results, however, show surprisingly good agreement with the experimental data, except at $\alpha=20°$ and $x/L=0.772$, where the grid resolution in the streamwise direction may not be enough to detect the delicate changes of the flow direction there.

In Figs. 6(a) and 6(b), the total velocity $|U|$ contours and the V-W vectors on the planes perpendicular to the body surface at $x/L=0.600$ and 0.772 are presented and compared with the experimental data. The upper- and lower half in each figure corresponds to the present results and experimental data, respectively. Note that the planes in the figures are different from the usual cross-plane sections that are perpendicular to the streamwise axis. At $\alpha=10°$ and $x/L=0.600$, the primary separation is observed, and it is developed to the vortex at $x/L=0.772$. The lower velocity region and the shape of $|U|$ contours agree well with the experimental data. At $\alpha=20°$ and $x/L=0.600$, the detached

vortex and incipient secondary separation are observed, and at *x/L=0.772* the vortex detached from the primary separation is already out of the range and the secondary separation is fully developed at $\phi=145°$. Again, the agreement between the present results and the data is not as good as that for $\alpha=10°$, as for the other flow variables.

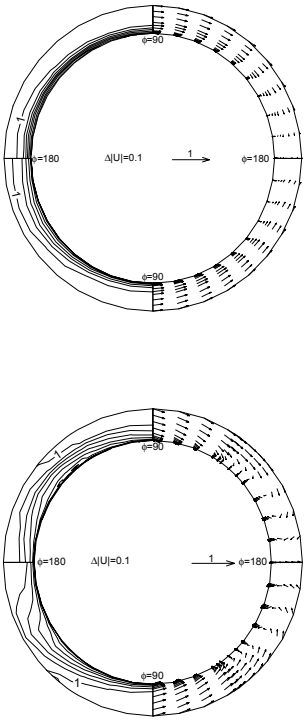

x/L=0.600(upper); *x/L=0.772* (lower)
Fig. 6(a) Total velocity contours and V-W vectors on the planes perpendicular to body surface at $\alpha=10°$
(upper half: present result,
lower half: experimental data[7]).

4. CONCLUDING REMARKS

Turbulent flow separations are investigated using an unstructured grid CFD method. Turbulent flow results are different from that of laminar flow in that the separation lines are moved leeward and backward and that the extent of vortices is smaller. The comparison with experimental data shows good agreement and confirms that the present method can be used to predict the 3D turbulent separated flows behind various 3D bodies.

Future work includes: application to more practical geometry such as various surface and underwater ships; application to unsteady turbulent separated flows such as the separation in maneuvering motion; and improvement of turbulence modeling for a better prediction in the region where strong turbulence anisotropy exists.

REFERENCES

(1) Simpson, R.L., "Three-dimensional Turbulent Boundary Layers and Separation," AIAA paper 95-0226, (1995).
(2) Roe, P.L., "Characteristic-based Schemes for the Euler Equations," Ann. Rev. Fluid Mech., vol.18, (1986).
(3) Spalart, P.R., and Allmaras, S.R., " A One-equation Turbulence Model for Aerodynamic Flows," AIAA paper 92-0439, (1992).
(4) Dacles-Mariani, J., Zilliac, G.G., Chow, J.S., and Bradshaw, P., "Numerical/Experimental Study of a Wingtip Vortex in the Near Field," AIAA J., vol.33, no.9, (1995).
(5) Hino, T., "A 3D Unstructured Grid Method for Incompressible Viscous Flows," J. Society of Naval Architects of Japan, vol.182, (1997).
(6) Rhee, S.H., and Hino, T., "Computational Investigation of 3D Turbulent Flow Separation around a Spheroid using an Unstructured Grid Method," J. Society of Naval Architects of Japan, vol.188, (2000).
(7) Chesnakas, C.J., and Simpson, R.L., "Detailed Investigation of the Three-dimensional Separation about a 6:1 Prolate Spheroid," AIAA J. vol.35, no.6, (1997).
(8) Matsumura, K., Tanaka, I., Oki, T., and Kishi, S., "On the Nonlinear Lift Characteristics of Slender Bodies at Incidence –Boundary Layer Separation and the Behavior of Vortex Sheets--," J. Society of Naval Architects of Japan, vol.154, (1983).
(9) Wetzel, T.G., Simpson, R.L., and Chesnakas, C.J., "Measurement of Three-dimensional Crossflow Separation," AIAA J. vol.36, no.4., (1998).

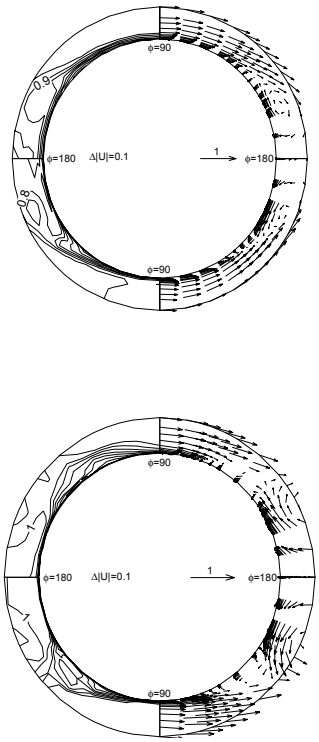

x/L=0.600(upper); *x/L=0.772* (lower)
Fig. 6(b). Total velocity contours and V-W vectors on the planes perpendicular to body surface at $\alpha=20°$
(upper half: present result,
lower half: experimental data[7]).